Efficient Implementation of a Quantum Algorithm in a Single Nitrogen-Vacancy Center of Diamond

Jingfu Zhang, Swathi S. Hegde, and Dieter Suter
Fakultät Physik, Technische Universität Dortmund, D-44221 Dortmund, Germany

(Received 19 November 2019; accepted 24 June 2020; published 14 July 2020)

Quantum computers have the potential to speed up certain problems that are hard for classical computers. Hybrid systems, such as the nitrogen-vacancy (NV) center in diamond, are among the most promising systems to implement quantum computing, provided the control of the different types of qubits can be efficiently implemented. In the case of the NV center, the anisotropic hyperfine interaction allows one to control the nuclear spins indirectly, through gate operations targeting the electron spin, combined with free precession. Here, we demonstrate that this approach allows one to implement a full quantum algorithm, using the example of Grover's quantum search in a single NV center, whose electron is coupled to a carbon nuclear spin.

DOI: 10.1103/PhysRevLett.125.030501

Introduction.—Storing and processing digital information in quantum mechanical systems has an enormous potential for solving certain computational problems that are intractable in classical computers [1,2]. Important examples of efficient algorithms that require quantum mechanical processors include Grover's quantum search [3] over an unsorted database and prime factorization using Shor's algorithm [4]. Hybrid systems consisting of different types of physical qubits, such as the nitrogen-vacancy (NV) center in diamond, appear promising for building quantum computers [5–9], since they combine useful properties of different types of qubits. The NV center [9–11], e.g., combines the long coherence time of the nuclear spins with the rapid operations possible on the electron spins. However, the benefits are limited by the fact that the coupling between the nuclear spins and the external control fields is 3–4 orders of magnitudes weaker than for the electron spins, which results in slow operations of the nuclear spins if the gates are implemented by control fields based on radio-frequency (rf) pulses [12,13].

The strategy of indirect control [14–25] can reduce this limitation. This approach does not require external control fields (rf pulses) acting directly on the nuclear spins. Instead, only microwave (MW) pulses acting on the electron spin are applied, combined with free precession under the effect of anisotropic hyperfine interactions between the electron and nuclear spins. In previous works, we used this approach for the implementation of basic operations like initialization of qubits and quantum gate operations, including a universal set of gates for quantum computing [24,25]. In these works, we could greatly improve the control efficiency, e.g., compared with approaches based on multiple dynamical decoupling cycles [19,20,22] or modulated pulses [14,16]: our elementary unitary operations consisted of only 2–3 rectangular MW pulses separated by delays.

Here, we apply this approach to the implementation of a full quantum algorithm, Grover's search algorithm [3], which is one of the milestones in the field of quantum information. In the task of finding one entry in an unsorted database, Grover's search algorithm scales with the size N of the database as $\mathcal{O}(\sqrt{N})$, while all classical algorithms scale as $\mathcal{O}(N)$. Grover's quantum search has been implemented in various physical systems, such as NMR [26–28], NV centers [12,29], trapped atomic ions [30,31], optics [32], and superconducting systems [33]. In this Letter, we implement it by indirect control, with only 4 MW pulses for the whole quantum search. The experimental results demonstrate the very high efficiency of the indirect control in implementing quantum computing.

Grover's quantum search.—Grover's search algorithm [3] can speed up the search of an unsorted database quadratically compared to the classical search. The algorithm starts by initializing the n-qubit quantum register to an equal superposition of all basis states,

$$|\Psi\rangle_{\text{in}} = \frac{1}{\sqrt{N}} \sum_{i=0}^{N-1} |i\rangle,$$

where $N = 2^n$ and $|i\rangle$ denote the basis states of the system, each of which maps to an item in the database. This state can be prepared by initializing all qubits into state $|0\rangle$ and then applying Hadamard gates ($H^{\otimes n}$) to each of them.

The algorithm then requires the repeated application of two operations D and I_t, where the oracle I_t implements a phase flip operation for the target state $|s_t\rangle$ but does not change any other state: $I_t = I - 2|s_t\rangle\langle s_t|$, where I is the

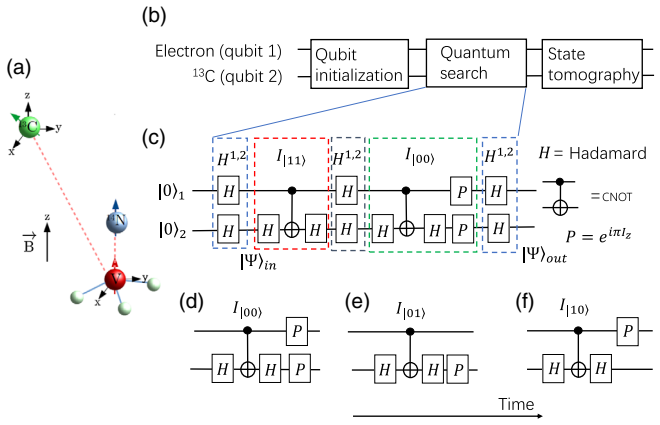

FIG. 1. (a) Structure of the NV system with the electron spin coupled to one ^{14}N and one ^{13}C nuclear spin. (b) Schematic representation of the experimental procedure, including the initialization, the quantum search, and the state tomography for determining the outcome, where (c) shows the gate sequence for searching the target state $|11\rangle$. $|\Psi\rangle_{\text{in}}$ denotes the equal superposition of all basis states. The output state $|\Psi\rangle_{\text{out}}$ is the target state $|11\rangle$. The circuits for the other target states $|00\rangle$, $|01\rangle$, $|10\rangle$ are obtained by replacing the phase flip operation $I_{|11\rangle}$ by $I_{|00\rangle}$, $I_{|01\rangle}$, $I_{|10\rangle}$, which can be implemented by the circuits shown in (d)–(f).

identity operator in the n-qubit system. D denotes a diffusion operation, and can be represented as $D = 2P - I = H^{\otimes n} I_{|00\ldots0\rangle} H^{\otimes n}$, where $|00\ldots0\rangle$ denotes the state of all qubits in $|0\rangle$ and $P = (\sum_{i,j=0}^{N-1} |i\rangle\langle j|)/N$. After applying $U = DI_t$ to $|\Psi\rangle_{\text{in}}$ m times, the system is in the state $|\Psi\rangle_{\text{out}} = U^m |\Psi\rangle_{\text{in}}$. In this state, the amplitude of the target state can approach 1 after $m \sim \mathcal{O}(\sqrt{N})$, while a classical search requires $\mathcal{O}(N)$ oracle operations.

Experimental protocol.—For the experimental implementation we used a diamond with 99.995% ^{12}C, and the concentration of substitutional nitrogen of < 10 ppb to minimize decoherence [34–36]. The experimental setup is presented in the Supplemental Material (SM) [37], which includes Refs. [38–41]. The experiment was performed at room temperature in a static magnetic field B of 14.8 mT along the symmetry axis of the NV center. The structure of the NV center with the coupled ^{14}N and ^{13}C nuclear spins is illustrated in Fig. 1(a). Here, we use a symmetry-adapted coordinate system, where the z axis is oriented along the NV axis, while the ^{13}C nucleus is located in the xz plane [42]. In this context, we focus on the subsystem where the ^{14}N is in the state $m_N = 1$. The relevant Hamiltonian for the electron and ^{13}C spins is then

$$\frac{\mathcal{H}_{e,C}}{2\pi} = DS_z^2 - (\gamma_e B - A_N) S_z - \gamma_C B I_z + A_{zz} S_z I_z + A_{zx} S_z I_x. \tag{1}$$

Here, S_z denotes the spin-1 operator for the electron and $I_{x/z}$ the ^{13}C spin-1/2 operators. The zero-field splitting is $D = 2.87$ GHz. $\gamma_{e/C}$ denotes the gyromagnetic ratios for the electron and ^{13}C spins, respectively. $A_N = -2.16$ MHz is the secular part of the hyperfine coupling between the electron and the ^{14}N nuclear spin [43–45], while A_{zz} and A_{zx} are the relevant components of the ^{13}C hyperfine tensor, which are $A_{zz} = -0.152$ MHz and $A_{zx} = 0.110$ MHz in the present system.

We select a 2-qubit system for implementing the quantum search by focusing on the subspace with the electron spin in $\{|0\rangle, |-1\rangle\}$ as qubit 1 and the ^{13}C spin as the second qubit. Our computational basis $\{|0\rangle, |1\rangle\}_1 \otimes \{|0\rangle, |1\rangle\}_2$ corresponds to the physical states $\{|0\rangle, |-1\rangle\}_e \otimes \{|\uparrow\rangle, |\downarrow\rangle\}_C$, where the states $|0\rangle$ and $|-1\rangle$ denote the eigenstates of S_z, $|\uparrow\rangle$ and $|\downarrow\rangle$ the eigenstates of I_z with eigenvalues of $1/2$ and $-1/2$, respectively. Figure 1(b) outlines the protocol for implementing the quantum search.

In the step of qubit initialization, we use a 4 μs, 0.5 mW pulse of 532 nm laser light to initialize the electron spin into the $m_S = 0$ state. Additional details of the setup are in the SM. Based on the initialized electron spin, we further polarize the ^{13}C spin by a combination of MW and laser pulses, and set the qubits into the pure state $|00\rangle$ [24,25]. Additional details are given in the SM.

The protocol for the actual quantum search is shown in Fig. 1(c) for the target state $|s_t\rangle = |11\rangle$. The circuits for the other target states $|00\rangle$, $|01\rangle$, and $|10\rangle$ are obtained by replacing the phase flip operation $I_{|11\rangle}$ by $I_{|00\rangle}$, $I_{|01\rangle}$, and $I_{|10\rangle}$, as shown in Figs. 1(d)–1(f), respectively.

To implement the actual search shown as Fig. 1(c), we considered sequences of MW pulses with constant MW and Rabi frequencies but variable durations and phases. The MW frequencies were resonant with the ESR transitions between the electron states $m_S = 0 \leftrightarrow m_S = -1$. The pulse durations, phases, and delays were used as variables in an optimization procedure based on optimal control (OC) theory [24,25,46] that maximizes the overlap between the operation generated by the sequence and the operation required by the quantum circuit of Fig. 1(c), which can reach unity in the ideal case [14,15,47].

The OC process has to balance several considerations. While it is helpful to use many pulses and therefore many degrees of freedom to optimize the theoretical fidelity of the gate operation, additional pulses also increase the total duration of the sequence and therefore the effect of decoherence (mainly from the electron spin in the present work), and the experimental imperfections also tend to increase with the number of pulses. We found sequences of 4 pulses and 5 delays to be a good compromise for all four target states, see details in SM.

To determine the state of the system after the search operation, we use the techniques developed in quantum state tomography [1,48], to reconstruct the populations or full quantum states. This requires a set of measurements applied to the output state $|\Psi\rangle_{\text{out}}$.

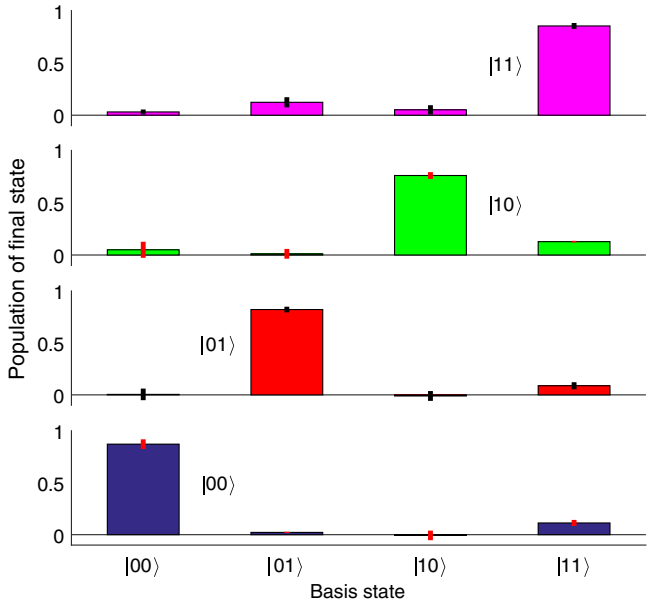

FIG. 2. Experimentally measured populations of the four basis states after the quantum search with the targets $|00\rangle$, $|01\rangle$, $|10\rangle$, and $|11\rangle$, as indicated in the panels. The error bars indicate 1 standard deviation, which was determined by repeating each experiment.

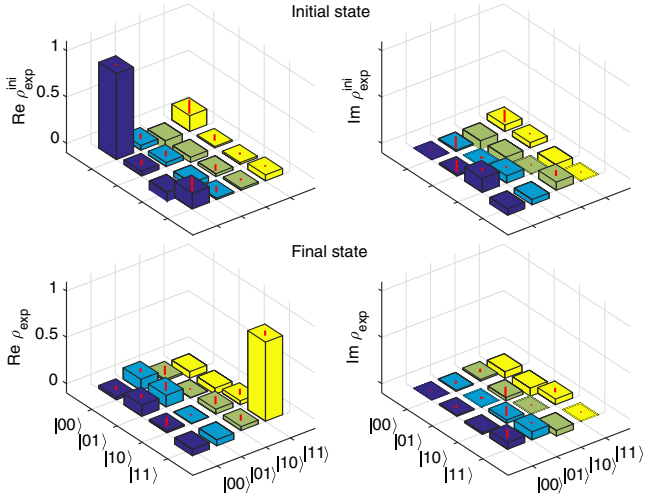

FIG. 3. Measured density matrices for the prepared initial state $|00\rangle$ (top) and for the state after the completion of the quantum search with target state $|11\rangle$ (bottom). The real and imaginary parts are shown in the left and right columns.

Experimental results.—Figure 2 illustrates the experimental results for the different target states. Here, we only show the populations obtained from partial tomography. The measured populations of the target states, or the probabilities of finding the target states, are 0.87 ± 0.05, 0.82 ± 0.03, 0.76 ± 0.03, and 0.85 ± 0.03 for the target states $|00\rangle$, $|01\rangle$, $|10\rangle$, and $|11\rangle$, with the sums of the populations 1.00 ± 0.03, 0.90 ± 0.03, 0.95 ± 0.06, and 1.06 ± 0.02, respectively. In each case the probability of finding the target state is much higher than the classical result of 0.25. In the ideal case, the population of the target state should be 1 and the others 0. The deviation of the sum of the populations for each case from the unity can be mainly attributed to imperfections in the tomography, which cause population leakage to the electron state $m_S = 1$. Second, the incomplete selectivity of the MW pulses leads to loss of population from the computational subspace. We estimate that this contribution is less than 0.027 in our experiments. The effects from the coupled ^{14}N spin can be decreased, e.g., by polarizing ^{14}N [49–55], where the polarization can be $> 98\%$ [49,55]. The details are presented in the SM.

Figure 3 shows the reconstruction of the full density matrices for the initial state and the search result for the target state $|11\rangle$. By calculating the fidelities as $F = \mathrm{Tr}\{\rho_{\mathrm{th}}\rho_{\mathrm{exp}}\}$, we obtained $F_{\mathrm{ini}} = 0.92 \pm 0.01$ and $F_{|11\rangle} = 0.85 \pm 0.03$ for the initial state and the final state after the quantum search. The loss of the fidelity in the quantum search can be attributed to the imperfection of the theoretical pulse sequence, the experimentally implemented sequence, and the experimentally implemented initial state including the state tomography, in the order of importance. The details of the error estimation are presented in the SM.

Discussion.—The OC efficiency can be improved by maximizing the angle between the different quantization axes of the nuclear spin for the different states of the electron spin [15]. The experimental fidelity might be improved further, e.g., by increasing the robustness with respect to fluctuations of the Rabi frequency (see examples in the SM, Sec. VII A), and increasing the Rabi frequency [24], e.g., in the case that the ^{14}N is polarized. Moreover, the choice of a more efficient optimal algorithm should be helpful [56,57]. To estimate the scalability of the OC scheme in larger systems, we use numerical simulation of systems with one electron spin and $n = 1, \ldots, 4$ ^{13}C spins. As examples, we use 3–4 MW pulses with 4–5 delays to implement the CNOT-like gates, where the electron spin (in the subspace $m_S = 0$ and $m_S = -1$) acts as the control qubit, while one ^{13}C spin is the target qubit. The target operation is chosen as $R_x^j(\pi) = e^{-i\pi I_x^j}$, where j indicates the target ^{13}C spin. The details are presented in the SM.

We investigate the dependence of the gate fidelity and duration on the number of the qubits in the system. The results are shown in Fig. 4, and the parameters for the pulse sequences are presented in the SM. The results show that the ^{13}C spin quantization axis orientation in the subspace $m_S = -1$, denoted as θ_- in Fig. 4(a), is a crucial factor in the optimization. The quality of the gate, here evaluated by the gate fidelity and duration, is degraded only marginally by the passive ^{13}C spins coupled to the electron. For example, for $j = 1$, with $\theta_- = 87°$, the gate fidelity is higher than 0.995, and the gate duration remains the range

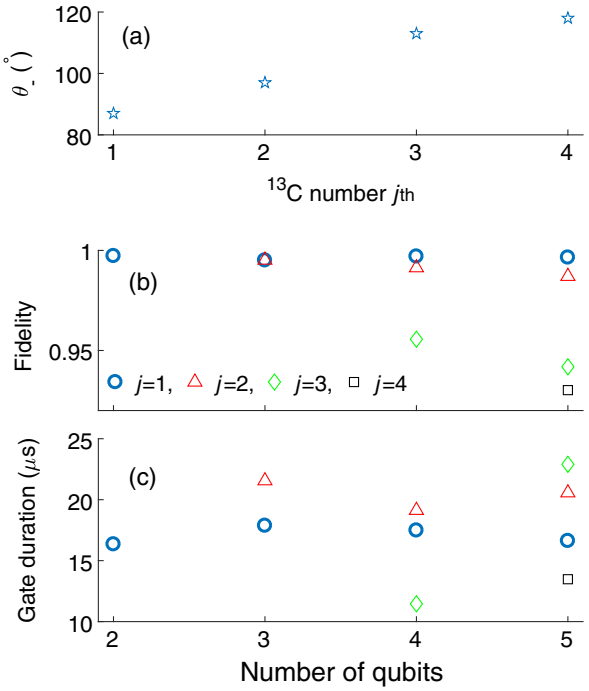

FIG. 4. (a) The quantization axis orientation of jth ^{13}C spin of the subspace $m_S = -1$ between z axis, the orientation of the subspace $m_S = 0$. (b),(c) Results by simulation of controlled-$R_x^j(\pi)$ (CNOT-like gates) in 2–5-qubit systems, respectively, where the electron spin is the control qubit, and $R_x^j(\pi) = e^{-i\pi I_x^j}$ with j indicating the affected ^{13}C spin. (b) and (c) show the gate fidelity and duration, respectively.

of 16–18 μs for up to 5 qubits. In other cases, with θ_- in the range of 97°–118°, we obtain fidelities in the range of 0.930–0.995, with gate durations of 11–23 μs. The fidelity can be improved further by increasing the number of MW pulses.

Since the CNOT gate can be combined with single-qubit gates to yield a universal set of gates [1,17], the method presented in this Letter represents a universal solution for implementing quantum computing.

Conclusion.—We have experimentally implemented Grover's quantum search algorithm in a hybrid quantum register in a single NV center in diamond by indirect control: control pulses were applied only to the electron spin, which has a much faster response time than the nuclear spins. In a 2-qubit system, we implemented 4 cases of the quantum search, in each of which one target state was searched. The whole procedure for demonstrating the quantum algorithm was implemented, including the preparation of the pure state, implementation of the quantum search and reconstruction of the output state. For each target state, the complete search algorithm was implemented with only 4 MW pulses. This corresponds to a significant reduction of the control cost compared with previous works. Further improvements should be possible by designing the pulse sequence robust against dephasing effects, or by combining the operations with dynamical decoupling techniques [13,58–60].

This project has received funding from the European Union's Horizon 2020 research and innovation programme under Grant agreement No. 828946. We thank Daniel Burgarth for helpful discussions.

The publication reflects the opinion of the authors; the agency and the commission may not be held responsible for the information contained in it.

[1] M. A. Nielsen and I. L. Chuang, *Quantum Computation and Quantum Information* (Cambridge University Press, Cambridge, England, 2000).
[2] J. Stolze and D. Suter, *Quantum Computing: A Short Course from Theory to Experiment*, 2nd ed. (Wiley-VCH, Berlin, 2008).
[3] L. K. Grover, Phys. Rev. Lett. **79**, 325 (1997).
[4] P. W. Shor, SIAM J. Comput. **26**, 1484 (1997).
[5] T. D. Ladd, F. Jelezko, R. Laflamme, Y. Nakamura, C. Monroe, and J. L. O'Brien, Nature (London) **464**, 45 (2010).
[6] M. Blencowe, Nature (London) **468**, 44 (2010).
[7] J. Cai, F. Jelezko, and M. B. Plenio, Nat. Commun. **5**, 4065 (2014).
[8] G. Kurizki, P. Bertet, Y. Kubo, K. Mølmer, D. Petrosyan, P. Rabl, and J. Schmiedmayer, Proc. Natl. Acad. Sci. U.S.A. **112**, 3866 (2015).
[9] D. Suter and F. Jelezko, Prog. Nucl. Magn. Reson. Spectrosc. **98–99**, 50 (2017).
[10] J. Wrachtrup and F. Jelezko, J. Phys. Condens. Matter **18**, S807 (2006).
[11] M. W. Doherty, N. B. Manson, P. Delaney, F. Jelezko, J. Wrachtrup, and L. C. L. Hollenberg, Phys. Rep. **528**, 1 (2013).
[12] T. van der Sar, Z. H. Wang, M. S. Blok, H. Bernien, T. H. Taminiau, D. M. Toyli, D. A. Lidar, D. D. Awschalom, R. Hanson, and V. V. Dobrovitski, Nature (London) **484**, 82 (2012).
[13] J. Zhang and D. Suter, Phys. Rev. Lett. **115**, 110502 (2015).
[14] J. S. Hodges, J. C. Yang, C. Ramanathan, and D. G. Cory, Phys. Rev. A **78**, 010303(R) (2008).
[15] N. Khaneja, Phys. Rev. A **76**, 032326 (2007).
[16] Y. Zhang, C. A. Ryan, R. Laflamme, and J. Baugh, Phys. Rev. Lett. **107**, 170503 (2011).
[17] P. Cappellaro, L. Jiang, J. S. Hodges, and M. D. Lukin, Phys. Rev. Lett. **102**, 210502 (2009).
[18] C. D. Aiello and P. Cappellaro, Phys. Rev. A **91**, 042340 (2015).
[19] T. H. Taminiau, J. J. T. Wagenaar, T. van der Sar, F. Jelezko, V. V. Dobrovitski, and R. Hanson, Phys. Rev. Lett. **109**, 137602 (2012).
[20] T. H. Taminiau, J. Cramer, T. van der Sar, V. V. Dobrovitski, and R. Hanson, Nat. Nanotechnol. **9**, 171 (2014).
[21] J. Casanova, Z.-Y. Wang, and M. B. Plenio, Phys. Rev. A **96**, 032314 (2017).

[22] F. Wang, Y.-Y. Huang, Z.-Y. Zhang, C. Zu, P.-Y. Hou, X.-X. Yuan, W.-B. Wang, W.-G. Zhang, L. He, X.-Y. Chang *et al.*, Phys. Rev. B **96**, 134314 (2017).
[23] G.-Q. Liu, H. C. Po, J. Du, R.-B. Liu, and X.-Y. Pan, Nat. Commun. **4**, 2254 (2013).
[24] J. Zhang, S. S. Hegde, and D. Suter, Phys. Rev. Applied **12**, 064047 (2019).
[25] S. S. Hegde, J. Zhang, and D. Suter, Phys. Rev. Lett. **124**, 220501 (2020).
[26] I. L. Chuang, N. Gershenfeld, and M. Kubinec, Phys. Rev. Lett. **80**, 3408 (1998).
[27] L. M. K. Vandersypen, M. Steffen, M. H. Sherwood, C. S. Yannoni, G. Breyta, and I. L. Chuang, Appl. Phys. Lett. **76**, 646 (2000).
[28] J. Zhang, X. Peng, N. Rajendran, and D. Suter, Phys. Rev. A **75**, 042314 (2007).
[29] Y. Wu, Y. Wang, X. Qin, X. Rong, and J. Du, npj Quantum Inf. **5**, 9 (2019).
[30] K.-A. Brickman, P. C. Haljan, P. J. Lee, M. Acton, L. Deslauriers, and C. Monroe, Phys. Rev. A **72**, 050306(R) (2005).
[31] C. Figgatt, D. Maslov, K. A. Landsman, N. M. Linke, S. Debnath, and C. Monroe, Nat. Commun. **8**, 1918 (2017).
[32] N. Bhattacharya, H. B. van Linden van den Heuvell, and R. J. C. Spreeuw, Phys. Rev. Lett. **88**, 137901 (2002).
[33] L. DiCarlo, J. M. Chow, J. M. Gambetta, L. S. Bishop, B. R. Johnson, D. I. Schuster, J. Majer, A. Blais, L. Frunzio, S. M. Girvin, and R. J. Schoelkopf, Nature (London) **460**, 240 (2009).
[34] K. D. Jahnke, B. Naydenov, T. Teraji, S. Koizumi, T. Umeda, J. Isoya, and F. Jelezko, Appl. Phys. Lett. **101**, 012405 (2012).
[35] T. Teraji, T. Taniguchi, S. Koizumi, Y. Koide, and J. Isoya, Appl. Phys. Express **6**, 055601 (2013).
[36] J. Zhang, J. H. Shim, I. Niemeyer, T. Taniguchi, T. Teraji, H. Abe, S. Onoda, T. Yamamoto, T. Ohshima, J. Isoya *et al.*, Phys. Rev. Lett. **110**, 240501 (2013).
[37] See Supplemental Material at http://link.aps.org/supplemental/10.1103/PhysRevLett.125.030501 for details of the NV setup, spin system, pulse sequences, error analysis, effects of ^{14}N in Grover's search, pure state preparation, and additional data for optimal control, which includes Refs. [38–41].
[38] L. Childress, M. V. Gurudev Dutt, J. M. Taylor, A. S. Zibrov, F. Jelezko, J. Wrachtrup, P. R. Hemmer, and M. D. Lukin, Science **314**, 281 (2006).
[39] J. Zhang, S. S. Hegde, and D. Suter, Phys. Rev. A **98**, 042302 (2018).
[40] L. M. K. Vandersypen and I. L. Chuang, Rev. Mod. Phys. **76**, 1037 (2005).
[41] J. Zhang, S. Saha, and D. Suter, Phys. Rev. A **98**, 052354 (2018).
[42] K. R. Rao and D. Suter, Phys. Rev. B **94**, 060101(R) (2016).
[43] C. S. Shin, M. C. Butler, H.-J. Wang, C. E. Avalos, S. J. Seltzer, R.-B. Liu, A. Pines, and V. S. Bajaj, Phys. Rev. B **89**, 205202 (2014).
[44] X.-F. He, N. B. Manson, and P. T. H. Fisk, Phys. Rev. B **47**, 8816 (1993).
[45] B. Yavkin, G. Mamin, and S. Orlinskii, J. Magn. Reson. **262**, 15 (2016).
[46] M. Mitchell, *An Introduction to Genetic Algorithms* (MIT Press, Cambridge, MA, 1998).
[47] D. D'Alessandro, *Introduction to Quantum Control and Dynamics* (Taylor and Francis, Boca Raton, FL, 2008).
[48] G. M. Leskowitz and L. J. Mueller, Phys. Rev. A **69**, 052302 (2004).
[49] N. Xu, Y. Tian, B. Chen, J. Geng, X. He, Y. Wang, and J. Du, Phys. Rev. Applied **12**, 024055 (2019).
[50] T. Chakraborty, J. Zhang, and D. Suter, New J. Phys. **19**, 073030 (2017).
[51] K. R. K. Rao, Y. Wang, J. Zhang, and D. Suter, Phys. Rev. A **101**, 013835 (2020).
[52] D. Pagliero, A. Laraoui, J. D. Henshaw, and C. A. Meriles, Appl. Phys. Lett. **105**, 242402 (2014).
[53] C. Zu, W.-B. Wang, L. He, W.-G. Zhang, C.-Y. Dai, F. Wang, and L.-M. Duan, Nature (London) **514**, 72 (2014).
[54] W.-B. Wang, C. Zu, L. He, W.-G. Zhang, and L.-M. Duan, Sci. Rep. **5**, 12203 (2015).
[55] J. Yun, K. Kim, and D. Kim, New J. Phys. **21**, 093065 (2019).
[56] X.-S. Yang, arXiv:2003.03776 [J. Comput. Sci. (to be published)].
[57] T. Weise, Global Optimization Algorithms—Theory and Application (2009) (electronic version available as http://www.it-weise.de/projects/bookNew.pdf).
[58] J. Zhang, A. M. Souza, F. D. Brandao, and D. Suter, Phys. Rev. Lett. **112**, 050502 (2014).
[59] A. M. Souza, G. A. Álvarez, and D. Suter, Phys. Rev. A **86**, 050301(R) (2012).
[60] D. Suter and G. A. Álvarez, Rev. Mod. Phys. **88**, 041001 (2016).